ACS SENSORS

Article

Cite This: ACS Sens. 2018, 3, 2152−2158

pubs.acs.org/acssensors

Pt-Functionalized PdO Nanowires for Room Temperature Hydrogen Gas Sensors

Hee-Jin Cho,[†] Vivian T. Chen,[‡] Shaopeng Qiao,[§] Won-Tae Koo,[†] Reginald M. Penner,*[,‡] and Il-Doo Kim*[,†]

[†]Department of Materials Science and Engineering, Korea Advanced Institute of Science and Technology (KAIST), Daejeon 34141, Republic of Korea

[‡]Department of Chemistry and [§]Department of Physics, University of California, Irvine, California 92697-2025, United States

Supporting Information

ABSTRACT: In this work, we prepared a well-aligned palladium oxide nanowire (PdO NW) array using the lithographically patterned Pd nanowire electrodeposition (LPNE) method followed by subsequent calcination at 500 °C. Sensitization with platinum (Pt) nanoparticles (NPs), which were functionalized on PdO NWs through a simple reduction process, significantly enhanced the detection capability of the Pt-loaded PdO NWs (Pt-PdO NWs) sensors toward hydrogen gas (H_2) at room temperature. The well-distributed Pt NPs, which are known chemical sensitizers, activated the dissociation of H_2 and oxygen molecules through the spillover effect with subsequent diffusion of these products to the PdO surface, thereby transforming the entire surface of the PdO NWs into reaction sites for H_2. As a result, at a high concentration of H_2 (0.2%), the Pt-PdO NWs showed an enhanced sensitivity of 62% (defined as $\Delta R/R_{air} \times 100\%$) compared to that (6.1%) of pristine PdO NWs. The Pt-PdO NWs exhibited a response time of 166 s, which was 2.68-fold faster than that of pristine PdO NWs (445 s). In addition, the Pt-PdO NWs responded to a very low concentration of H_2 (10 ppm) with a sensitivity of 14%, unlike the pristine PdO NWs, which did not exhibit any response at that concentration. These outstanding results are mainly attributed to a homogeneous decoration of Pt NPs on the surface of well-aligned PdO NWs. In this work, we demonstrated the potential suitability of Pt-PdO NWs as a highly sensitive H_2 sensing layer at room temperature.

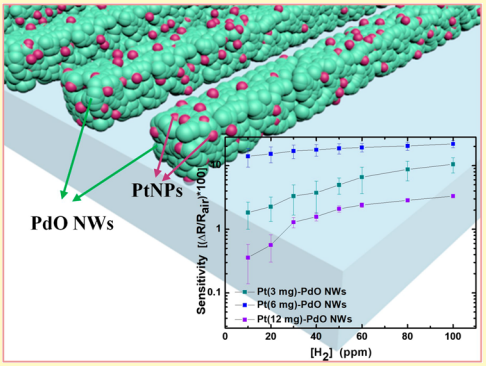

KEYWORDS: *hydrogen chemical sensors, PdO nanowires, LPNE, Pt catalyst, electrodeposition*

Hydrogen gas (H_2) has been widely used as a renewable energy source due to its vast abundance, high combustion efficiency, and outstanding gravimetric energy density. As interest in H_2 increases, leakage and detection of H_2 become very important issues because H_2 has a lower flammability limit of 4%. Unfortunately, H_2 is a less perceivable gas because it is tasteless, colorless, and odorless. Therefore, there is a growing need for an accurate H_2 detecting sensor, and various H_2 sensors have been reported.[1,2] In particular, chemiresistive-type sensors have been intensively studied as a promising H_2 sensor due to their small size, simple fabrication, low cost, and easily interpreted results.[3] Among materials for chemiresistive sensing, Pd has been extensively studied as a promising H_2 sensing material because its resistance immediately increases by forming PdH_x under H_2 ambient. Favier et al. first reported electrodeposited Pd mesowire arrays for a fast H_2 sensor at room temperature,[4] and later, Yang et al. demonstrated that Pd nanowires (NWs) exhibited superior H_2 sensing properties compared to those of Pd films.[5] Further, Li et al. reported enhanced response speed by modifying the Pd nanowires with Pt at an elevated temperature (316 K).[6]

Alternative chemiresistive sensing materials include the semiconductor metal oxides (SMOs) such as SnO_2,[7,8] ZnO,[9] and WO_3.[10] The working principle of SMOs, which possess good chemical stability and high reproducibility, involves a simple resistance change. When SMOs are exposed to target molecules, their base resistance is changed due to modulation of the electron depletion layer. However, most SMO-based sensors suffer from high operating temperature (150−400 °C), which is linked to safety concerns and power consumption. Although there have been attempts to develop SMO-based hydrogen sensors that can operate at room temperature, some issues including low sensitivity, sluggish response behavior, and slow recovery speed remain unresolved.[11,12] In this respect, in this work, a three-pronged strategy has been employed to develop advanced sensors that can practically detect H_2 gas at room temperature: (i) selection of PdO as a sensing material, (ii) use of aligned one-dimensional NW array, and (iii) catalytic Pt nanoparticle (NP) functionalization. Among several SMOs, a p-type palladium oxide (PdO) has not been extensively studied as a sensing material.[13] Chang et al.

Received: July 26, 2018
Accepted: September 28, 2018
Published: September 28, 2018

DOI: 10.1021/acssensors.8b00714
ACS Sens. 2018, 3, 2152−2158

Scheme 1. Synthesis Process of Pt Nanoparticle (NP)-Decorated PdO NWs (Pt-PdO NWs): (a) Glass Substrate, (b) Formation of Ni Layer onto Glass Substrate, (c) Spin-Coated Photoresist (PR) Layer on Ni Layer, (d) Nanowires (NWs) Patterned Using a UV Lamp and a Photomask, (e) Electrodeposition of Pd in the Trenches Under the PR Layer, (f) Formation of Well-Aligned Pd NWs, (g) Synthesis of Well-Aligned PdO NWs, and (h) Decoration of Pt NPs on PdO NWs (Pt-PdO NWs).

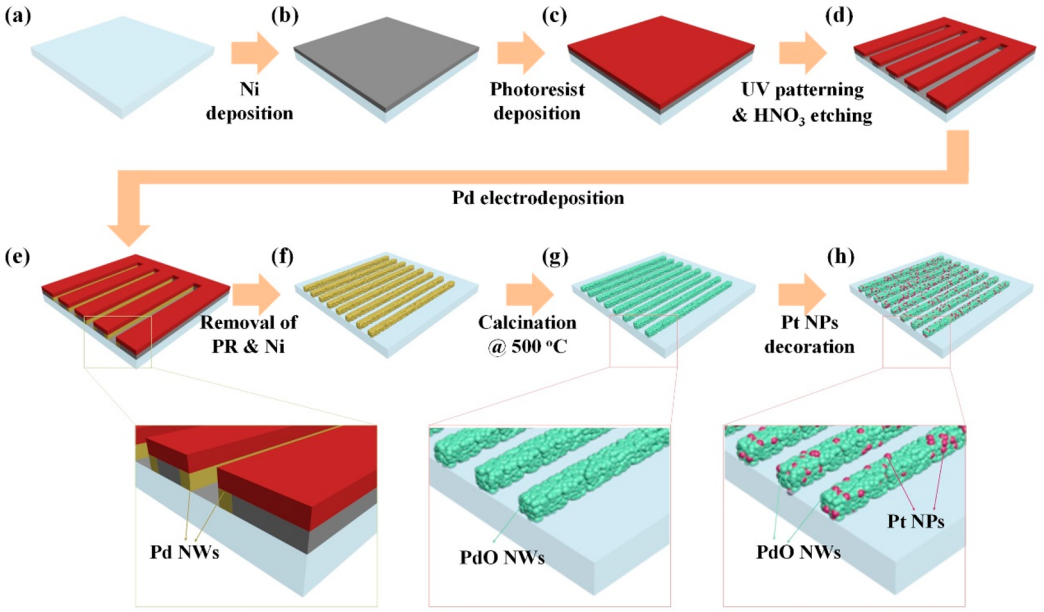

investigated the H_2 detection capability of the PdO film in the temperature range of 25−250 °C, where the best sensing properties were achieved at 100 °C, and Lee et al. reported the PdO film-based H_2 sensors operated at room temperature. In the latter case, however, the sensor was tested under ambient N_2 balance and exhibited a low limit of detection (~2%).[14−16] Because the sensing reactions occur on the surfaces of SMOs, to achieve the improved sensing properties, one-dimensional fibrous SMO structures with high surface area are the most desired morphologies. In particular, the entire surfaces of well-aligned one-dimensional NWs can act as gas-accessible reaction sites because there is no overlap of NWs. In addition, functionalization of SMOs with catalytic noble metal NPs such as Pt,[1,6] Pd,[17,18] and Au,[19,20] is essential for improving the sensing characteristics. Typically, the catalytic effect can be maximized by optimizing the amount of noble catalytic NPs and their homogeneous distribution onto SMOs surfaces.[21] Several researchers have reported on the functionalization of SMOs by catalytic NPs, which are synthesized via polyol method[22] or soft templating routes such as apoferritin,[23,24] chitosan,[25] and metal−organic frameworks,[26] which control the size of the NPs and prevent agglomeration. Although such soft templates were effective in controlling size of NPs and preventing the severe agglomeration of NPs during synthetic processing, the fabrication processes are rather complicated and require longer times. A simple reduction process of a metal precursor in solution for catalytic functionalization is an alternative process to address these issues.

In this work, well-aligned one-dimensional Pd NWs are fabricated through the facile lithographically patterned nanowire electrodeposition (LPNE) method,[27] followed by calcination at 500 °C to form p-type PdO NWs. Afterward, PdO NWs are decorated with catalytic platinum NPs (Pt NPs) through a simple and fast reduction of the platinum precursor in solution.[28] The one-dimensional morphology endows the well-aligned PdO NWs with high sensitivity toward H_2 at room temperature, especially, upon functionalization of their surfaces with Pt catalysts.

EXPERIMENTAL SECTION

Chemical. Optical glass slides (1 in × 1 in) were purchased from Fisher and used as substrates. Acetone and ethanol were also purchased from Fisher. Nickel (Ni) and gold (Au) pellets (5 N purity) were purchased from Kurt J. Lesker. Palladium chloride ($PdCl_2$, 99.999%), ethylenediaminetetraacetic acid (EDTA, 99.995%), potassium hexachloroplatinate(IV) (K_2PtCl_6, 99.99%), ethylene glycol, and butylamine were purchased from Sigma-Aldrich. A positive photoresist (Shipley S1808) and a developer (Shipley MF-319) were purchased from Microchem Corporation. H_2 gas (2%) and dry air were sourced from Airgas, whereas H_2 gas (1000 ppm) was sourced from Praxair.

Synthesis of PdO NWs. Aligned Pd NW arrays were fabricated using the conventional LPNE process.[5] Ni film, 40 nm in height, was deposited onto the optical glass slide through thermal evaporation. A positive photoresist (S1808) was spin-coated onto the Ni film-coated glass substrate at 2500 rpm for 80 s followed by soft baking at 90 °C for 30 min. The photoresist layer was patterned using a photolithographic contact mask, a photolithographic alignment fixture (Newport model 97436, i-line, 500 W, and 2.3 s) and a UV light source, resulting in the fabrication of well-aligned 450 arrayed NWs with a 4 μm pitch. The photoresist coated on the Ni film/glass substrate was developed in developer solution (MF-319) for 20 s and rinsed with Millipore water. For creating a slight undercut beneath the photoresist, the exposed Ni was etched by immersing the developed substrate in 0.8 M nitric acid solution for 6 min. The Ni edge was used as a working electrode to electrodeposit Pd (using a Gamry Series G 300) under −0.9 V vs saturated calomel reference electrode (SCE) with a Pt foil counter electrode for 900 s. For etching the residual Ni layer, the photoresist was rinsed off with acetone and then the substrate was immersed in 0.8 M nitric acid solution for 5 min followed by rinsing with Millipore water and drying in ambient air. Then, the Pd NW array was oxidized during calcination at 500 °C in air for 1 h, resulting in the formation of p-type PdO NW array.

DOI: 10.1021/acssensors.8b00714
ACS Sens. 2018, 3, 2152−2158

Synthesis of Pt-Decorated PdO NWs. To chemically sensitize PdO NWs by a catalyst, we functionalized the PdO NWs with Pt NPs via a simple reduction process. A solution was prepared by dissolving potassium hexachloroplatinate(IV) in 25 mL of ethylene glycol. The amount of Pt NPs was controlled by dissolving the appropriate amount of the Pt precursor in the solution (3, 6, and 12 mg of K_2PtCl_6). The glass slide with patterned PdO NWs was placed into the solution at a constant temperature of 75 °C. Then, 5 mM butylamine was added to the solution and stirred for 20 min. The obtained Pt-decorated PdO NWs on the glass substrate were rinsed with ethanol and Millipore water and dried for 12 h at 40 °C using a hot plate.

Characterization. Pristine PdO NWs and Pt-decorated PdO NWs (Pt-PdO NWs) were characterized by field-emission scanning electron microscopy (FE-SEM, Magellan 400 XHR system, FEI) operated at 10 kV. Energy-dispersive X-ray spectroscopy (EDS) mapping images were obtained from the same SEM equipped with an EDS detector (80 mm^2, Aztec software, Oxford Instruments). Grazing incidence X-ray diffraction pattern (XRD, Ultima III, Rigaku) analysis was conducted with Cu Kα radiation (λ = 1.5418 Å) for analysis of each crystal structure.

Sensor Fabrication and Evaluation of Gas Sensing Performance. The Au electrodes were patterned onto the prepared PdO NWs and Pt-sensitized PdO NWs (Pt-PdO NWs) through thermal evaporation of Au followed by spin coating and soft baking of the S1808 photoresist. The chromium (Cr) layer was deposited below the Au layer to increase its adhesion onto glass. The photoresist layer was then patterned and subsequently etched to fabricate the Au electrodes spaced at 20 μm. The variation in resistance was investigated using a four-probe system with a source meter (model 2400, Keithley Instruments) and a multimeter (model 2000, Keithley Instruments). The H_2 concentration was adjusted using two mass flow controllers (MFC) (model 1479A, MKS Inc.) through mixing with dry air. All H_2 sensing measurements were conducted at room temperature.

RESULTS AND DISCUSSION

Fabrication of Sensing Materials. Scheme 1 presents an illustration for fabrication steps of Pt-PdO NWs; synthetic process flow of PdO NWs using LPNE route[27] and decoration of PdO NWs with Pt NPs using a simple reduction method. First, Ni and the photoresist (PR) were sequentially deposited onto glass substrate through thermal evaporation and spin coating, respectively. The well-aligned NWs were patterned using the contact mask, UV light, and the developer. After UV patterning, Pd was electrodeposited within the narrow trenches that were formed upon intentional overetching of the Ni layer under the PR film using nitric acid (see details in Experimental Section). The well-aligned Pd NWs with a pitch of 4 μm were obtained by removing residual PR and Ni using acetone and nitric acid, respectively. For acquiring the well-crystallized PdO NWs, the Pd NWs were calcined at 500 °C in air for 1 h. After then, the glass slide with PdO NWs was immersed into a solution containing ethylene glycol and the Pt precursor. Then, butylamine was added to reduce the Pt precursor to Pt NPs.[29] Finally, Pt-sensitized PdO NWs were formed, and the H_2 sensing performance using Pt-PdO NWs was investigated.

Microstructural Characterization. The microstructures of pristine PdO NWs and Pt-sensitized PdO NWs were observed using SEM. As shown in Figure 1a, the low magnification SEM image confirmed the well-aligned PdO NWs. The higher magnification image showed that the PdO NWs (150 nm in diameter) were polycrystalline and consisted of densely packed PdO NPs (Figure 1b). The PdO NWs and Pt-PdO NWs had nearly the same diameter. However, the Pt-PdO NWs exhibited more densely packed surface morphology while maintaining the dimensions of NWs (Figure 1c and d).

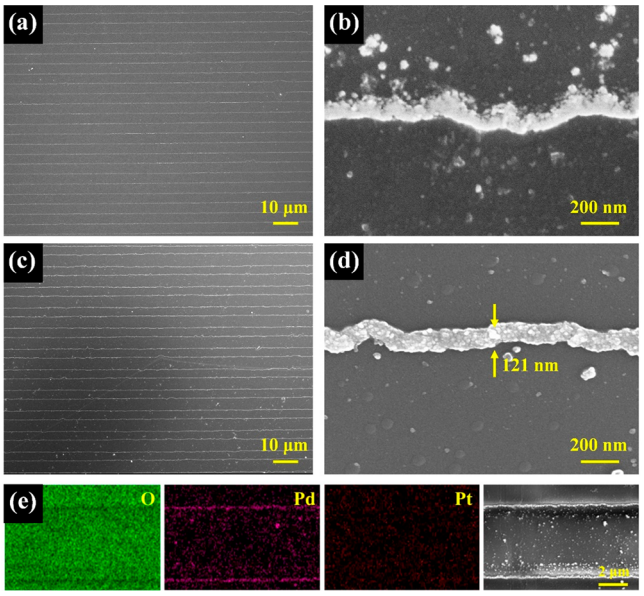

Figure 1. Morphology observation using SEM: (a) pristine PdO NWs, (b) magnified image of (a), (c) Pt-PdO NWs, (d) magnified image of (c), and (e) energy-dispersive spectroscopy (EDS) images of Pt-PdO NWs.

The existence of Pd, O, and Pt elements in Pt-PdO NWs was clearly confirmed through EDS analysis (Figure 1e).

The EDS linescan analysis was performed using SEM to further determine the morphology of the Pt-PdO NWs. To control the loading amount of Pt NPs on PdO NWs, we used three different concentration of Pt precursors, i.e., 3, 6, and 12 mg. Although elemental Pt was barely detectable in the Pt (3 mg)-PdO NWs, the Pt line showed island-like morphology in Pt (6 mg)-PdO NWs (Figure S1a). In addition, Pt NPs were also deposited onto bare glass during the reduction process. In the Pt (12 mg)-PdO NWs, the Pt NPs were intermittently interconnected (Figure S1b) due to the agglomeration caused by excessive Pt precursor loading. On the other hand, elemental Pd was observed only on PdO NWs, as expected. Because both the PdO NWs and glass substrate contain oxygen species, elemental O existed in all regions.

The crystalline structure of PdO NWs and Pt-PdO NWs were investigated using grazing incidence X-ray diffraction (XRD) analysis (Figure S2). In the XRD result, four peaks were observed at 33.6, 33.9, 41.9, and 54.8° corresponding to (002), (101), (110), and (112) planes of PdO, respectively. The big shoulder before 30−38° was attributed to the glass slide because it was composed of amorphous SiO_2. The peaks associated with Pt species such as metallic Pt, or oxidized Pt, were not observed in XRD data due to the very small quantities of Pt NPs on PdO NWs. X-ray photoelectron spectroscopy (XPS) analysis was performed to further investigate the chemical bonding states of Pt and Pd (Figure 2). The Pd largely existed in Pd^{2+} state with a binding energy of 337.1 eV,[24] which is well matched with the XRD results for the PdO phase. The remaining fraction of Pd existed in the Pd^{4+} state. In the case of Pt, the metallic Pt^0 and oxidized Pt^{2+} coexisted.[28] The XPS data indicated that some metallic Pt oxidized to Pt^{2+} state because Pt^{2+} has a relatively lower reduction potential (1.18 eV) than that of Pd^{4+} (1.288 eV),[30] which means that the Pd^{4+} ion is more likely to be reduced

DOI: 10.1021/acssensors.8b00714
ACS Sens. 2018, 3, 2152−2158

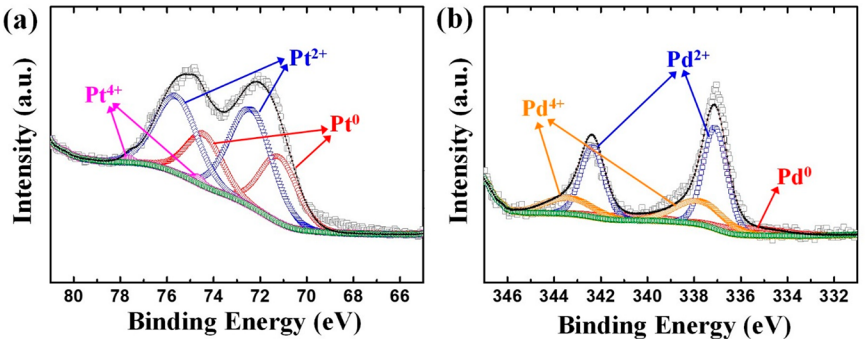

Figure 2. XPS spectra of (a) Pt and Pd in Pt (6 mg)-PdO NWs.

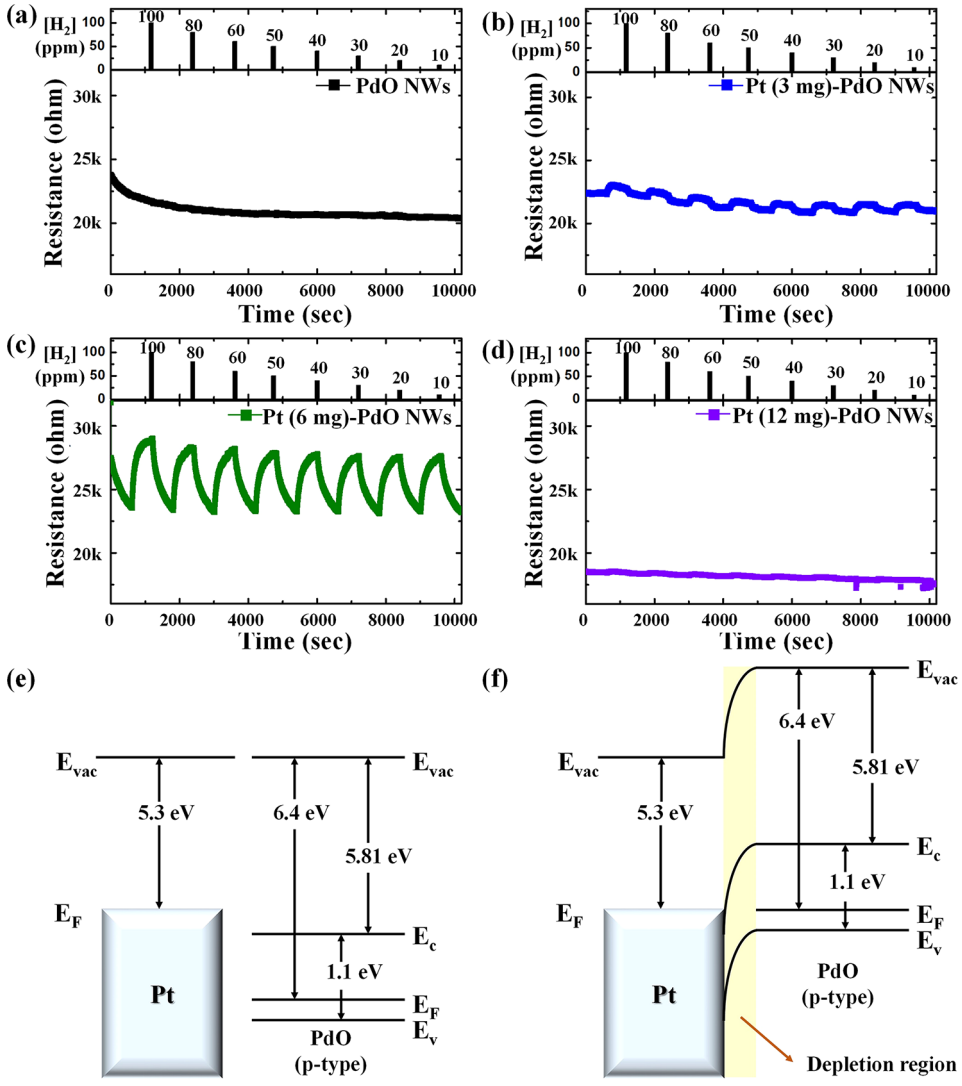

Figure 3. Dynamic resistance transients of (a) pristine PdO NWs, (b) Pt (3 mg)-PdO NWs, (c) Pt (6 mg)-PdO NWs, and (d) Pt (12 mg)-PdO NWs for a range of 10−100 ppm of H_2, and the band diagram of Pt and PdO (e) work functions of Pt and PdO, (f) when Pt and PdO are in contact.

than Pt^{2+}. Therefore, Pt^{2+} as well as metallic Pt^0 were observed in the XPS results.

Hydrogen Sensing Properties. For investigating the H_2 sensing characteristics, the performance of the pristine PdO NWs and three different Pt-PdO NWs (i.e., decorated with 3, 6, and 12 mg of Pt precursor) was evaluated toward H_2 at room temperature in ambient air. The two parallel Au electrodes (spaced at 20 μm) were used to detect the changes in resistance. The H_2 sensing measurement was conducted using low (10−100 ppm) and high (0.1−0.2%) concentration of H_2. The concentration of H_2 was controlled by mass flow controllers (MFCs) through dilution with air, and allowing the gas mixture to flow onto the sensors for 10 min at each concentration. The dynamic resistance transients of pristine

DOI: 10.1021/acssensors.8b00714
ACS Sens. 2018, 3, 2152−2158

PdO NWs and Pt-PdO NWs are shown in Figure 3 and Figure S3. The pristine PdO NWs exhibited small resistance changes toward H_2 in the concentration range of 0.1−0.2%, where the sensitivity toward 0.2% H_2 was 6% (Figure S3a), which is a higher sensitivity value than that of Pd NWs reported elsewhere.[31] However, no resistance changes were observed in pristine PdO NWs at very low concentrations (10−100 ppm) of H_2 (Figure 3a).

On the other hand, introducing a small amount of Pt NPs onto PdO NWs slightly increased the response to H_2, which indicated that Pt NPs can improve the sensitivity to H_2 (Figure 3b). Furthermore, a higher amount (6 mg) of Pt NPs onto PdO NWs resulted in a tremendously improved sensitivity toward H_2 (Figure 3c and Figure S3b). However, the response to H_2 decreased with decoration of PdO NWs with an excessive amount of Pt NPs (Figure 3d). In terms of the sensing mechanism, PdO, which is a p-type SMO,[15] has a hole accumulation layer at the surface. An upward band bending occurred in the vicinity of the PdO surface because the adsorbed oxygen species withdraws electrons from forming the hole accumulation layer (Figure S4a). Consequently, an electrical current can flow along the hole accumulation layer on the surface of PdO with a relatively low resistance in ambient air. When PdO is exposed to reducing gases such as H_2, the trapped electrons are restored to the valence band of the PdO during the reactions of adsorbed oxygen with the reducing gases, resulting in a recombination of electrons and holes. In this way, the amount of electrical current in PdO decreases by the thinning of the hole accumulation layer, resulting in a relatively higher resistance of PdO (Figure S4b).[31] In the process, a partial reduction of Pd^{4+} to metallic Pd occurs following a restoration of the electrons into PdO due to its poor stability and high reduction potential (Figure S5). Reversibly, the resistance of PdO is recovered during re-exposure to air, allowing for the readsorption of oxygen. Therefore, PdO detects H_2 through resistance modulation.[32] The base resistances of Pt (3 mg)-PdO NWs and Pt (6 mg)-PdO NWs increased when they were exposed to ambient air. The increase in base resistance can be explained by the formation of Schottky contacts at the interfaces of Pt NPs and PdO NWs (Figure 3e and f). For the Fermi levels to be aligned at equilibrium, the hole accumulation layer of PdO thinned owing to the flow of electrons from metallic Pt, which was effectuated by the higher work function (6.4 eV)[33] of PdO compared to that of metallic Pt (5.3 eV).[34] Therefore, the base resistance increased linearly with the amount of Pt NPs.

Pt is a very well-known chemical sensitizer capable of providing more adsorbed oxygen species onto PdO NWs through the spillover effect.[24,35] A larger amount of adsorbed oxygen can offer more reactions for H_2 on the PdO surface, thereby exhibiting a higher response. Furthermore, in the case of a p-type semiconductor, the contribution of chemical sensitization becomes more significant to accelerate sensing reactions due to lower charge carrier concentration. Therefore, the functionalization of Pt NPs onto PdO NWs significantly enhances the H_2 sensing characteristics.[31] However, excessive amounts of Pt NPs lead to agglomeration into larger clusters that cover almost the entire surface of PdO NWs. In this case, the larger reactive surface toward H_2 is provided by Pt NPs than PdO NWs, thus resulting in lower sensitivity. Furthermore, the interfaces between agglomerated Pt NPs increased in Pt (12 mg)-PdO NWs compared to those in pristine PdO NWs. Accordingly, the Pt (12 mg)-PdO NWs showed lower base resistance. In addition, when excessive amounts of Pt NPs are decorated, oxygen can be dissociatively adsorbed onto Pt NPs and becomes negatively charged (O_2^-). The adsorbed oxygen can induce positive charges at the interfaces of Pt NPs and PdO NWs, thereby lowering the base resistance.[16,36]

The sensitivity was defined in terms of the resistance ratio, i.e., $\Delta R/R_{air} \times 100$ (%), where ΔR is the difference between the resistance in air (R_{air}) and in reducing ambient (R_{gas}) (Figure 4a). The Pt (6 mg)-PdO NWs exhibited the best

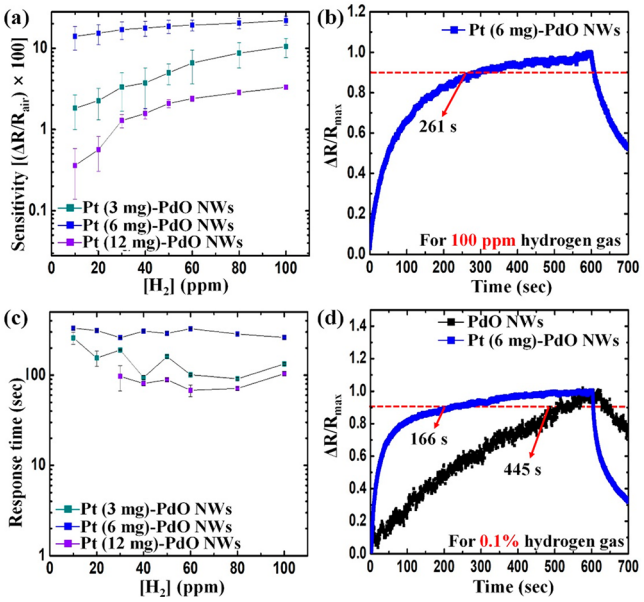

Figure 4. (a) Sensitivity of Pt-PdO NWs in the range of 10−100 ppm of H_2, and (b) the normalized curve of response for Pt-PdO NWs for 100 ppm of H_2. (c) Response time of Pt-PdO NWs in the range of 10−100 ppm of H_2, and (d) normalized curve of Pt (6 mg)-PdO NWs and pristine PdO NWs for 0.1% H_2.

sensitivity at all concentrations (23% toward 100 ppm) and displayed 6.61- and 2.09-fold enhanced sensitivities compared to those of Pt (12 mg)-PdO NWs and Pt (3 mg)-PdO NWs, respectively. In terms of response time, the Pt (6 mg)-PdO NWs showed a rapid response time of 261 s and 166 s to 100 ppm and 0.1% H_2 gas, respectively (Figure 4b and d). The Pt (12 mg)-PdO NWs showed a faster response time, whereas the Pt (6 mg)-PdO NWs exhibited much higher sensitivity. Furthermore, in the case of Pt (12 mg)-PdO NWs, it was impossible to calculate the response time at concentrations below 30 ppm because the Pt (12 mg)-PdO NWs exhibited almost no response to such concentrations. The lower sensitivity and rapid response speed of Pt (12 mg)-PdO NWs is attributed to the excessive agglomeration of Pt NPs that blocked the reactive sites on PdO NWs owing to quick dissociation of oxygen and H_2 molecules by Pt NPs.[6] The catalyst has an optimum density that facilitates the spillover effect over the entire surface of PdO, resulting in the formation of an effective oxygen delivery system for reactions with H_2.[37] Therefore, in this work, the well-aligned PdO NWs with the optimum amount of Pt NPs demonstrated the feasibility of superior H_2 sensors at room temperature.

DOI: 10.1021/acssensors.8b00714
ACS Sens. 2018, 3, 2152−2158

CONCLUSIONS

In this work, we fabricated well-aligned PdO NWs as superior room temperature H_2 sensors through functionalization of PdO NWs with Pt NPs. The well-aligned PdO NWs, which were synthesized using the LPNE method and subsequent calcination at 500 °C, demonstrated high sensitivity to very low concentration (0.1−0.2%) of H_2 compared to that of Pd NWs. On the contrary, pristine PdO NWs did not display a noticeable response to H_2 concentrations below 100 ppm. For its sensitivity to be improved further, Pt NPs were decorated onto PdO NWs with a simple reduction process that greatly improved the sensitivity toward H_2. The Pt (6 mg)-decorated PdO NWs exhibited a high sensitivity of 14% at 10 ppm of H_2. Furthermore, functionalization with Pt NPs improved the response time ∼3.16-fold upon exposure to 0.1% H_2. This work demonstrated a simple fabrication of the metal oxide NWs and catalytic functionalization through the LPNE method and reduction process, respectively. In addition, the superior H_2 detection capabilities of the NWs were proved at room temperature in ambient air.

ASSOCIATED CONTENT

Supporting Information

The Supporting Information is available free of charge on the ACS Publications website at DOI: 10.1021/acssensors.8b00714.

Element line scanning by field-emission scanning electron microscopy, X-ray diffraction patterns of PdO NWs and Pt-PdO NWs, dynamic resistance transient of PdO-based sensors in the range of 0.1−0.2% hydrogen, energy band diagram of PdO in air and H_2, and XPS spectra of Pt and Pd after exposure to H_2 (PDF)

AUTHOR INFORMATION

Corresponding Authors

*E-mail: idkim@kaist.ac.kr.
*E-mail: rmpenner@uci.edu.

ORCID

Reginald M. Penner: 0000-0003-2831-3028
Il-Doo Kim: 0000-0002-9970-2218

Notes

The authors declare no competing financial interest.

ACKNOWLEDGMENTS

This work was supported by the National Research Foundation of Korea (NRF), grant No. 2014R1A4A1003712 (BRL Program). This work was also supported by Wearable Platform Materials Technology Center (WNC) funded by National Research Foundation of Korea (NRF) Grant of the Korean Government (MSIP) (No. 2016R1A5A1009926). This work was also supported by Multi-Ministry Collaborative R&D Program (Development of Techniques for Identification and Analysis of Gas Molecules to Protect Against Toxic Substances) through the National Research Foundation of Korea (NRF) funded by KNPA, MSIT, MOTIE, ME, NFA (2017M3D9A1073501). R.M.P., V.T.C., and S.Q. acknowledge funding from the National Science Foundation of the United States, contract CBET 1803314.

REFERENCES

(1) Wang, S.-C.; Shaikh, M. O. A room temperature H_2 sensor fabricated using high performance Pt-loaded SnO_2 nanoparticles. *Sensors* **2015**, *15* (6), 14286−14297.

(2) Penner, R. M. A nose for hydrogen gas: fast, sensitive H_2 sensors using electrodeposited nanomaterials. *Acc. Chem. Res.* **2017**, *50* (8), 1902−1910.

(3) Gu, H.; Wang, Z.; Hu, Y. Hydrogen gas sensors based on semiconductor oxide nanostructures. *Sensors* **2012**, *12* (5), 5517−5550.

(4) Favier, F.; Walter, E. C.; Zach, M. P.; Benter, T.; Penner, R. M. Hydrogen sensors and switches from electrodeposited palladium mesowire arrays. *Science* **2001**, *293* (5538), 2227−2231.

(5) Yang, F.; Kung, S. C.; Cheng, M.; Hemminger, J. C.; Penner, R. M. Smaller is faster and more sensitive: The effect of wire size on the detection of hydrogen by single palladium nanowires. *ACS Nano* **2010**, *4* (9), 5233−5244.

(6) Li, X.; Liu, Y.; Hemminger, J. C.; Penner, R. M. Catalytically activated palladium@ platinum nanowires for accelerated hydrogen gas detection. *ACS Nano* **2015**, *9* (3), 3215−3225.

(7) Yin, X.-T.; Tao, L. Fabrication and gas sensing properties of Au-loaded SnO_2 composite nanoparticles for low concentration hydrogen. *J. Alloys Compd.* **2017**, *727*, 254−259.

(8) Li, H.-H.; He, Y.; Jin, P.-P.; Cao, Y.; Fan, M.-H.; Zou, X.; Li, G.-D. Highly selective detection of trace hydrogen against CO and CH_4 by Ag/Ag_2O-SnO_2 composite microstructures. *Sens. Actuators, B* **2016**, *228*, 515−522.

(9) Kumar, M.; Singh Bhati, V.; Ranwa, S.; Singh, J.; Kumar, M. Pd/ZnO nanorods based sensor for highly selective detection of extremely low concentration hydrogen. *Sci. Rep.* **2017**, *7* (1), 236.

(10) Choi, S.-J.; Chattopadhyay, S.; Kim, J. J.; Kim, S.-J.; Tuller, H. L.; Rutledge, G. C.; Kim, I.-D. Coaxial electrospinning of WO_3 nanotubes functionalized with bio-inspired Pd catalysts and their superior hydrogen sensing performance. *Nanoscale* **2016**, *8* (17), 9159−9166.

(11) Fields, L.; Zheng, J.; Cheng, Y.; Xiong, P. Room-temperature low-power hydrogen sensor based on a single tin dioxide nanobelt. *Appl. Phys. Lett.* **2006**, *88* (26), 263102.

(12) Gao, M.; Cho, M.; Han, H. J.; Jung, Y. S.; Park, I. Palladium-decorated silicon nanomesh fabricated by nanosphere lithography for high performance, room temperature hydrogen sensing. *Small* **2018**, *14* (10), 1703691.

(13) Ryabtsev, S. V.; Shaposhnik, A. V.; Samoylov, A. M.; Sinelnikov, A. A.; Soldatenko, S. A.; Kuschev, S. B.; Ievlev, V. M. Thin films of palladium oxide for gas sensors. *Dokl. Phys. Chem.* **2016**, *470*, 158−161.

(14) Chiang, Y.-J.; Li, K.-C.; Lin, Y.-C.; Pan, F.-M. A mechanistic study of hydrogen gas sensing by PdO nanoflake thin films at temperatures below 250° C. *Phys. Chem. Chem. Phys.* **2015**, *17* (5), 3039−3049.

(15) Lee, Y. T.; Lee, J. M.; Kim, Y. J.; Joe, J. H.; Lee, W. Hydrogen gas sensing properties of PdO thin films with nano-sized cracks. *Nanotechnology* **2010**, *21* (16), 165503.

(16) Chiang, Y.-J.; Pan, F.-M. PdO nanoflake thin films for CO gas sensing at low temperatures. *J. Phys. Chem. C* **2013**, *117* (30), 15593−15601.

(17) Pandey, P.; Wilson, N.; Covington, J. Pd-doped reduced graphene oxide sensing films for H_2 detection. *Sens. Actuators, B* **2013**, *183*, 478−487.

(18) Nikfarjam, A.; Fardindoost, S.; Iraji zad, A. Fabrication of Pd doped WO_3 nanofiber as hydrogen sensor. *Polymers* **2013**, *5* (1), 45−55.

(19) Wang, Y.; Zhao, Z.; Sun, Y.; Li, P.; Ji, J.; Chen, Y.; Zhang, W.; Hu, J. Fabrication and gas sensing properties of Au-loaded SnO_2 composite nanoparticles for highly sensitive hydrogen detection. *Sens. Actuators, B* **2017**, *240*, 664−673.

(20) Chava, R. K.; Oh, S.-Y.; Yu, Y.-T. Enhanced H_2 gas sensing properties of Au@ In_2O_3 core−shell hybrid metal−semiconductor heteronanostructures. *CrystEngComm* **2016**, *18* (20), 3655−3666.

DOI: 10.1021/acssensors.8b00714
ACS Sens. 2018, 3, 2152−2158

(21) Hwang, I.-S.; Choi, J.-K.; Woo, H.-S.; Kim, S.-J.; Jung, S.-Y.; Seong, T.-Y.; Kim, I.-D.; Lee, J.-H. Facile control of C_2H_5OH sensing characteristics by decorating discrete Ag nanoclusters on SnO_2 nanowire networks. *ACS Appl. Mater. Interfaces* **2011**, *3* (8), 3140−3145.
(22) Bulemo, P. M.; Cho, H.-J.; Kim, N.-H.; Kim, I.-D. Mesoporous SnO_2 nanotubes via electrospinning−etching route: highly sensitive and selective detection of H_2S molecule. *ACS Appl. Mater. Interfaces* **2017**, *9* (31), 26304−26313.
(23) Cho, H.-J.; Kim, S.-J.; Choi, S.-J.; Jang, J.-S.; Kim, I.-D. Facile synthetic method of catalyst-loaded ZnO nanofibers composite sensor arrays using bio-inspired protein cages for pattern recognition of exhaled breath. *Sens. Actuators, B* **2017**, *243*, 166−175.
(24) Kim, S. J.; Choi, S. J.; Jang, J. S.; Cho, H. J.; Koo, W. T.; Tuller, H. L.; Kim, I. D. Exceptional high-performance of Pt-based bimetallic catalysts for exclusive detection of exhaled biomarkers. *Adv. Mater.* **2017**, *29* (36), 1700737.
(25) Rampino, A.; Borgogna, M.; Blasi, P.; Bellich, B.; Cesàro, A. Chitosan nanoparticles: preparation, size evolution and stability. *Int. J. Pharm.* **2013**, *455* (1−2), 219−228.
(26) Koo, W.-T.; Choi, S.-J.; Kim, S.-J.; Jang, J.-S.; Tuller, H. L.; Kim, I.-D. Heterogeneous sensitization of metal−organic framework driven metal@ metal oxide complex catalysts on an oxide nanofiber scaffold toward superior gas sensors. *J. Am. Chem. Soc.* **2016**, *138* (40), 13431−13437.
(27) Menke, E.; Thompson, M.; Xiang, C.; Yang, L.; Penner, R. Lithographically patterned nanowire electrodeposition. *Nat. Mater.* **2006**, *5* (11), 914−919.
(28) Jang, J.-S.; Kim, S.-J.; Choi, S.-J.; Kim, N.-H.; Hakim, M.; Rothschild, A.; Kim, I.-D. Thin-walled SnO_2 nanotubes functionalized with Pt and Au catalysts via the protein templating route and their selective detection of acetone and hydrogen sulfide molecules. *Nanoscale* **2015**, *7* (39), 16417−16426.
(29) Wang, Q.; Zhang, Y.; Zhou, Y.; Zhang, Z.; Xu, Y.; Zhang, C.; Sheng, X. Synthesis of dendrimer-templated Pt nanoparticles immobilized on mesoporous alumina for p-nitrophenol reduction. *New J. Chem.* **2015**, *39* (12), 9942−9950.
(30) William, M. H.; Lide, D.; Bruno, T. *CRC handbook of chemistry and physics*; CRC Press: Boca Raton, FL, USA, 2011; pp 8−21.
(31) Barsan, N.; Simion, C.; Heine, T.; Pokhrel, S.; Weimar, U. Modeling of sensing and transduction for p-type semiconducting metal oxide based gas sensors. *J. Electroceram.* **2010**, *25* (1), 11−19.
(32) Koo, W.-T.; Qiao, S.; Ogata, A. F.; Jha, G.; Jang, J.-S.; Chen, V. T.; Kim, I.-D.; Penner, R. M. Accelerating Palladium Nanowire H_2 Sensors Using Engineered Nanofiltration. *ACS Nano* **2017**, *11* (9), 9276−9285.
(33) Zhang, L.; Jaroniec, M. Toward designing semiconductor-semiconductor heterojunctions for photocatalytic applications. *Appl. Surf. Sci.* **2018**, *430*, 2−17.
(34) Kumar, A.; Katiyar, R. S.; Scott, J. F. Novel room temperature multiferroics for random access memory elements. *IEEE Trans. Sonics Ultrtason.* **2010**, *57* (10), 2237−2242.
(35) Jang, B.-H.; Landau, O.; Choi, S.-J.; Shin, J.; Rothschild, A.; Kim, I.-D. Selectivity enhancement of SnO_2 nanofiber gas sensors by functionalization with Pt nanocatalysts and manipulation of the operation temperature. *Sens. Actuators, B* **2013**, *188*, 156−168.
(36) Chiang, Y.-J.; Lee, K.-C.; Pan, F.-M. Effects of Pt decoration on the CO sensing reaction mechanism of PdO nanoflakes thin films. *J. Phys. Chem. C* **2015**, *119* (30), 17278−17287.
(37) Kolmakov, A.; Klenov, D.; Lilach, Y.; Stemmer, S.; Moskovits, M. Enhanced gas sensing by individual SnO_2 nanowires and nanobelts functionalized with Pd catalyst particles. *Nano Lett.* **2005**, *5* (4), 667−673.

DOI: 10.1021/acssensors.8b00714
ACS Sens. 2018, 3, 2152−2158